Snowfall increase counters glacier demise in Kunlun Shan and Karakoram

Remco J. de Kok[1], Philip D.A. Kraaijenbrink[1], Obbe A. Tuinenburg[2], Pleun N.J. Bonekamp[1], Walter W. Immerzeel[1]

5   [1]Department of Physical Geography, Utrecht University, Utrecht, PO Box 80115, 3508 TC, The Netherlands
[2]Copernicus Institute of Sustainable Development, Utrecht University, Utrecht, PO Box 80115, 3508 TC, The Netherlands

Correspondence to: Remco J. de Kok (r.j.dekok@uu.nl)

Abstract. Glaciers in High Mountain Asia provide an important water resource for communities downstream and they are markedly impacted by global warming, yet there is a lack in understanding of the observed glacier mass balances and their

10   spatial variability. In particular, the glaciers in the western Kunlun Shan and Karakoram ranges (WKSK) show neutral to positive mass balances despite global warming. Using models of the regional climate and glacier mass balance, we reproduce the observed patterns of glacier mass balance in High Mountain Asia of the last decades. We show that low temperature sensitivities of glaciers and an increase in snowfall, for a large part caused by increases in evapotranspiration from irrigated agriculture, result in positive mass balances in WKSK. The pattern of mass balances in High Mountain Asia can thus be

15   understood from the combination of changes in climatic forcing and glacier properties, with an important role for irrigated agriculture.

1. Introduction

Glaciers in High Mountain Asia (HMA, see Fig. 1) show a very diverse response to the changing climate. Most glaciers are losing mass, as expected, but surprisingly, glaciers are stable or growing in a region northwest of the Tibetan plateau, a

20   phenomenon dubbed the Karakoram anomaly (Hewitt, 2005). Recent studies have mapped glacier mass losses and velocity changes in detail and have shown that the regions of largest glacier growth and acceleration are the Kunlun Shan and parts of the Pamir, with the glaciers in Karakoram being close to a steady state (Brun, Berthier, Wagnon, Kääb, & Treichler, 2017; Dehecq et al., 2019; J. Gardelle, Berthier, Arnaud, & Kääb, 2013; Julie Gardelle, Berthier, & Arnaud, 2012; Kääb, Treichler, Nuth, & Berthier, 2015; Lin, Li, Cuo, Hooper, & Ye, 2017). Part of the mass balance variability seems correlated to differences

25   in the temperature sensitivity, i.e. the change of mass balance for a certain change in temperature, of the glaciers (Sakai & Fujita, 2017), but this alone cannot explain why some glaciers are actually growing.
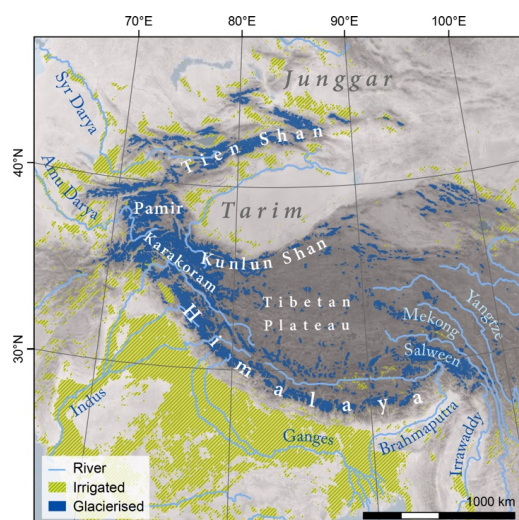
Figure 1: Map of study area. Irrigated areas (from GMIA (Siebert et al., 2010)) and glacierised areas (from RGI 6.0 (Pfeffer et al., 2014)) are indicated.

30

Suggested causes of the Karakoram anomaly include an increase in winter snowfall (Cannon, Carvalho, Jones, & Bookhagen, 2014; Kapnick, Delworth, Ashfaq, Malyshev, & Milly, 2014; J. Norris, Carvalho, Jones, & Cannon, 2015; Jesse Norris, Carvalho, Jones, & Cannon, 2018), summertime cooling (Bocchiola & Diolaiuti, 2013; Forsythe, Fowler, Li, Blenkinsop, &

35 Pritchard, 2017; Fowler & Archer, 2006; Khattak, Babel, & Sharif, 2011; Ul Hasson, Böhner, & Lucarini, 2017), and an increase in summertime precipitation and clouds due to irrigation in the agricultural regions adjacent to the Kunlun Shan and Pamir (de Kok, Tuinenburg, Bonekamp, & Immerzeel, 2018). So far, these hypotheses have only tried to explain the Karakoram anomaly in qualitative terms, identifying possible climatic conditions that could lead to glacier growth. None of these have yet been able to directly reproduce the observed pattern of glacier mass balances in HMA directly by showing the

40 response of the glaciers to the historic climatic forcing. Here, we simulate glacier mass balances using modelled time series of temperature and snowfall from a regional climate model to reproduce the pattern of observed mass balances in HMA, and to more deeply understand the underlying causes.

2

2. Methods

2.1 Regional climate model

45

Irrigation can influence the regional and global climate (Cook, Shukla, Puma, & Nazarenko, 2015; Lee, Sacks, Chase, & Foley, 2011; Lobell, Bonfils, & Faurès, 2008; Puma & Cook, 2010; Sacks, Cook, Buenning, Levis, & Helkowski, 2009). Since the regions surrounding HMA host the largest irrigated areas in the world, e.g. the Indo-Gangetic Plain (see Fig. 1), irrigation potentially influences the regional climate in HMA (Cai, Luo, He, Zhang, & Termonia, 2019; de Kok et al., 2018). However,

50 available re-analysis datasets do not fully include irrigation, and generally have a relatively coarse spatial resolution. Hence, we downscaled ERA-Interim (Dee et al., 2011) re-analysis data using the Weather Research and Forecasting model (WRF, Skamarock & Klemp, 2008) to obtain a high-resolution climate dataset between 1980-2010 for High Mountain Asia. We artificially applied irrigation to the surface by adding a precipitation term each time step, with a rate that is determined per month. The amount of irrigation applied per grid cell was based on the monthly water demand, which indicates the amount of

55 irrigation needed to compensate evapotranspiration, that was calculated by PCR-GLOBWB (van Beek & Bierkens, 2008; van Beek, Wada, & Bierkens, 2011; Van der Esch et al., 2017; Y. Wada, Wisser, & Bierkens, 2014; Yoshihide Wada et al., 2011). In this way, the irrigation amount is not easily overestimated, as could be the case when e.g. soil moisture would be kept constant. In reality, insufficient water might be available to meet the predicted demand, whereas inefficient irrigation will result in a larger water gift than predicted.

60

We used WRF, version 3.8.1, to downscale ERA-Interim data to a resolution of 20x20 km, with 50 vertical levels. Settings are nearly identical to our previous work (de Kok et al., 2018), and are shown in Table 1. Additionally, we now use grid nudging of the upper 35 vertical levels for horizontal wind, temperature, and humidity, as opposed to only forcing the model at the boundary in our previous study. The values of the nudging parameters have been found to perform well in similar studies

65 (Collier & Immerzeel, 2015; Otte, Nolte, Otte, & Bowden, 2012), and are: 0.001, 0.001, and 0.00005 s^{-1} for horizontal winds, temperature and water vapour, respectively.

Table 1: Physics modules and assumptions used in WRF.

Module	Setting
Radiation	RRTMG scheme (Iacono et al., 2008)
Microphysics	Morrison scheme (Morrison et al., 2009)
Cumulus	Kain-Fritsch (new Eta) scheme (Kain, 2004)
Planetary boundary layer	YSU scheme (Hong, Noh, & Dudhia, 2006)

Atmospheric surface layer	MM5 Monin-Obukhov scheme (Beljaars, 1995; Dyer & Hicks, 1970; Paulson, 1970; Webb, 1970; Zhang & Anthes, 1982)
Land surface	Noah-MP (Niu et al., 2011)
Top boundary condition	Rayleigh damping
Diffusion	Calculated in physical space
Nudging	Grid-point u, v, T, q above level 15

70

Annual concentrations of CO_2, CH_4, and N_2O are derived from NOAA (Dlugokencky, Lang, Mund, Crotwell, & Thoning, 2018) and AGAGE (Prinn et al., 2000) data, as aggregated by the European Environment Agency (www.eea.europa.eu, accessed March 2018), and are kept constant throughout each year. We used a 10-day spin-up for each month and run each month separately to be able to include a different irrigation amount each month. Monthly initialisation of the snow cover,

75 surface and soil temperature, and surface moisture was taken from GLDAS 2.0 (Rodell et al., 2004) monthly mean values. We checked convergence between months for temperature and precipitation and they agreed within a few percent for all selected points.

2.2 Glacier model

To assess the response of the glaciers to the atmospheric forcing, we employ a glacier mass balance gradient model
80 (Kraaijenbrink, Bierkens, Lutz, & Immerzeel, 2017). The model assumes a calibrated mass balance gradient along the glacier, and includes parameterisations for the effects of supraglacial debris on the surface mass balance and the downslope mass flux. We modelled all individual glaciers in HMA larger than 0.4 km^2 (n=33,587) transiently for the period 1980-2010 (Kraaijenbrink et al., 2017). For ease of comparison with published observations, we select only those larger than 2 km^2 for the final analysis, which represent 95% of the glacier volume in HMA. Initial mass balance conditions in 1980 were set to be

85 stable, using ERA-Interim data to locally calibrate the mass balance gradient of each glacier, while all other initial and reference conditions as described in the original study (Kraaijenbrink et al., 2017) were maintained. To modulate the mass balance gradient of the glacier over time, we applied annual precipitation changes derived from annual changes in WRF snowfall and temperature changes determined from annual changes in WRF melt season temperatures, i.e. when average daily temperature is above -5 °C. A threshold value of 0 °C did not significantly change the glacier mass balance results for most of HMA, but

90 meant that temperature changes for the coldest points could not be determined, since they are always below 0 °C. We did not take into account whether the WRF grid point was glacierised or not. To reduce potential biases imposed by spurious reference conditions, the reference for both deltas was taken to be the average of the first six modelling years, i.e. 1980-1985. We performed three separate glacier model runs to evaluate the attribution of snow and temperature to the glacier mass changes in our model, forced by: (1) precipitation and temperature, (2) only temperature, and (3) only snow. To illustrate the temperature

4

95   and precipitation sensitivity of the glaciers, we also performed calculations using a fixed temperature or snowfall trend for all
of HMA, with the other variable kept constant.

2.3 Moisture tracking

Our moisture tracking model (Tuinenburg, Hutjes, & Kabat, 2012) follows the moisture associated with precipitation
100   backwards in time to determine where the moisture first enters the atmosphere. It therefore establishes a direct causal link
between evapotranspiration and precipitation downwind. For the moisture tracking, we clustered locations that have similar
climates in terms of seasonality, since these will likely also have similar moisture sources. For the clustering, we used the
monthly mean values of precipitation, horizontal wind fields at 400 hPa, and 2m-temperatures, with means subtracted and
divided by the standard deviations, to perform a k-means clustering using 13 clusters. We performed the clustering with
105   different numbers of clusters and found 13 to give reasonably-sized, yet distinct areas, while also being close to the knee in
the total distance away from the cluster means. We perform the tracking on two of these clusters, indicated in Fig. 11, which
are close geographically, but have contrasting snowfall trends.

We perform the moisture tracking by releasing moisture parcels from the target area at random positions within the area and
110   advecting them backwards in time using interpolated wind fields on fixed pressure levels. The amount of evaporation A (mm)
that contributes to the precipitation in the target area, at a given location x,y and time step t, depends on the evapotranspiration
ET (mm), the amount of water in the parcel W_{parcel} (mm), the fraction of water in the parcel that evaporated from the source
S_{target}, and the total precipitable water in the column TPW (mm):

115    $$A_{x,y,t} = \mathrm{ET}_{x,y,t} \frac{W_{parcel,t} S_{target,t}}{\mathrm{TPW}_{x,y,t}} \quad , \tag{1}$$

The amount of water in the parcel is then updated every time step, including the precipitation P that adds to the parcel when
moving back in time.

120    $$W_{parcel,t-1} = W_{parcel,t} + \left(P_{x,y,t-1} - \mathrm{ET}_{x,y,t-1}\right) \frac{W_{parcel,t}}{TPW_{x,y,t-1}} \tag{2}$$

The fraction if precipitation in the target area that originates from a certain source area is then updated as follows:

$$S_{target,t-1} = \frac{S_{target,t} W_{parcel,t} - A_{x,y,t-1}}{W_{parcel,t-1}} \tag{3}$$

125

We track the parcel until either less than 1% of the target precipitation is tracked to a source area, or the tracking time is more than 30 days.

130   Within the WRF domain, the parcels are advected and the moisture budget is calculated using the WRF wind fields and water fluxes. When a parcel gets within one degree of the edge of the WRF domain, there is a gradual linear change to a use of ERA-Interim reanalysis data to ensure continuous movement of the air parcels over the domain edge. Within one degree distance from the domain edge, the values used to do the moisture tracking are a combination of the WRF and ERA-Interim values: y_{int} = $d*y_{WRF} + (1-d)*y_{ERA}$, where d is the distance to the edge. Outside of the WRF domain, the ERA-Interim values are used.

135   We noted that the surface moisture flux in ERA-Interim is on average 50% higher than in WRF, resulting in a higher mean and standard deviation of the moisture sources outside the WRF domain. Unfortunately, this systematic offset between the two datasets cannot be easily remediated. Although this will not change the spatial patterns of the moisture source trends in a major way, the absolute values of the trends will be lower in the WRF domain than outside. The trends in the Tarim basin will hence be underestimated with respect to regions such as the Caspian Sea and the Junggar basin.

140

2.4 Statistics

Pearson correlation coefficients are calculated using the vectors of annual or seasonal mean values. The trends shown in Figs. 2 and 4 are the slopes from linear fits to the annual mean vectors.

3. Results

145   ### 3.1 Validation and comparison

Any attempt to understand the Karakoram anomaly is greatly hampered by the almost complete lack of *in situ* meteorological data in WKSK. The rare weather stations in the region are often situated at relatively low elevation, or in urban environments, and poorly represent the high mountain climate. Furthermore, different types of precipitation datasets seem to greatly underestimate the precipitation in mountainous terrain (Immerzeel, Wanders, Lutz, Shea, & Bierkens, 2015; Ménégoz, Gallée,

150   & Jacobi, 2013; Palazzi, Von Hardenberg, & Provenzale, 2013). These complications imply that any meteorological dataset, including reanalysis datasets, are associated with relatively large fundamental errors in WKSK, which prevents reliable validation of any model of WKSK, such as the one presented in here. Nevertheless, we compared our WRF output with data of the region around WKSK, to ensure that the WRF output is a reasonable representation of the regional climate between 1980-2010.

155

We collected meteorological station data from GHCN (Lawrimore et al., 2011) (accessed June 2019), and selected those that have at least 20 years of full data between 1980-2010. Correlations between the annual variations in annual mean temperatures and mean temperatures between May-September are given in Fig. 2. They show generally very high correlations, with a lowest value of 0.5 (corresponding to p = 0.005). This implies that, despite many of these stations being situated in urban environments, the interannual variability is very well reproduced in WRF.

160

Figure 2: Pearson correlations between 1980-2010 time series of station data and nearest WRF grid for annual mean temperatures (a), May-September temperatures (b). The 2000 m-contour is indicated by a solid line

165

The stations in Fig. 2 closest to WKSK are almost exclusively in very arid regions, with a significant fraction of snowfall, making comparisons of precipitation very uncertain. Fig. 3 shows the correlation between time series of July precipitation, to limit the effect of snowfall, for the stations with monthly precipitation larger than 20 mm. The interannual variations are not represented by WRF as well as they are for temperature, but still show reasonable correlations for most stations, with values around 0.6.
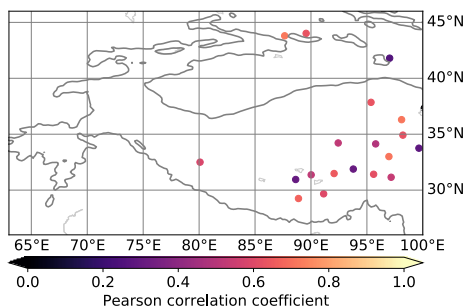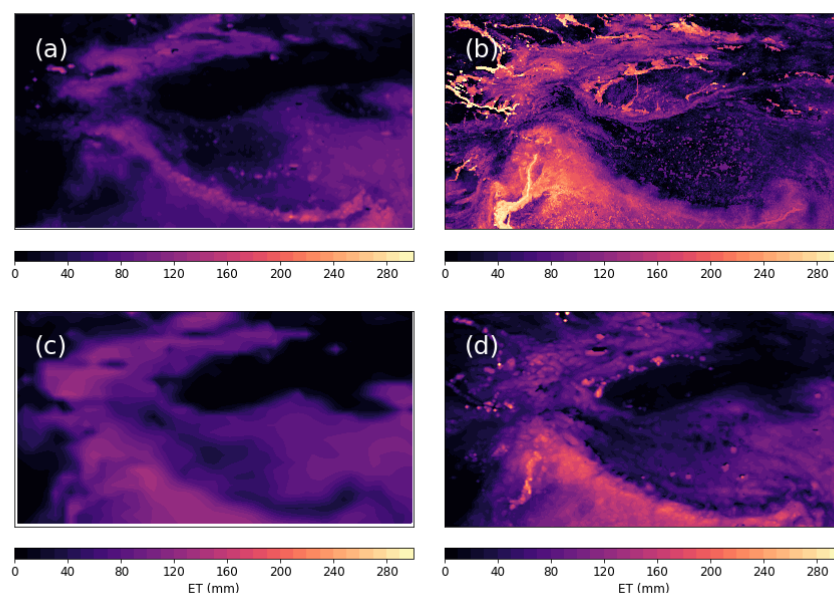
170

Figure 3: As Fig. 2, but for July precipitation.

7

175   Another parameter that is important in our model is evapotranspiration. It cannot be directly measured remotely, but there are several datasets that calculate it from other remotely sensed products, either directly or through data assimilation. These datasets vary greatly, as we illustrate in Fig. 4 for July 2010. We show evapotranspiration from GLEAM v 3.3a (Martens et al., 2017; Miralles, Gash, Holmes, De Jeu, & Dolman, 2010), which assimilates various soil moisture, temperature, radiation, and precipitation products. Furthermore, we show SSEBop (Senay, 2018) data, which uses MODIS temperatures directly,

180   ERA-Interim reanalysis data, and our WRF output. On the inner Tibetan Plateau, the WRF output agrees very well with the GLEAM data. Interannual variations also match very well between WRF and GLEAM in snow-free areas on the Tibetan Plateau, with correlation coefficients above 0.5 for time series between 1980-2010. However, it is clear that GLEAM does not represent the irrigated areas well, with unrealistically low evapotranspiration in heavily irrigated arid regions in July. In contrast, SSEBop shows very high evapotranspiration in the irrigated regions. The WRF output better resembles SSEBOP in

185   those areas, although generally has lower extremes, which are only in part explained by the difference in spatial resolution. ERA-Interim does not show the irrigation as prominently as WRF or SSEBop, but has a generally higher evapotranspiration values over unirrigated areas, such as the Tibetan Plateau. In general, the WRF simulated evapotranspiration is intermediate compared to the other datasets with plausible spatial patterns and magnitudes.

Figure 4: Evapotranspiration for July 2010 from GLEAM (a), SSEBop (b), ERA-Interim (c), and WRF (d). Mean values for the plotted domains are: 44 mm (a), 46 mm (b), 57 mm (c), and 59 mm (d).

3.2 Climatic trends

To get an impression how glaciers might have been affected by changes in the climate, we illustrate the trends for two relevant variables: the 2m-temperature in the melt season and the annual snowfall (Fig. 5, see also Fig. 6 for representative time series). For each grid point, the melt season was defined as the months where the mean daily temperature is above -5 °C, since for these months temperatures will likely be above freezing at least part of the time. A threshold value of 0 °C slightly increased the positive temperature trends at lower elevations in WKSK, but meant no trends for the highest elevations could be determined. The trends show that temperatures in the melt season have generally increased, with the northern part of the domain heating up the fastest and parts of the Indo-Gangetic Plain, Kunlun Shan, Karakoram, and the Tibetan Plateau showing only modest increases in temperature. The snowfall trends have a very different pattern, with most of the Tibetan Plateau showing an increase and the western and southern mountain ranges, such as the Himalaya and the Hindu-Kush, showing a decrease in snowfall. The increase in snowfall in WKSK mainly occurs in May, June, and September, whereas the decrease of snowfall in southwestern HMA occurs mainly in March (see Fig. 7 for region averages).
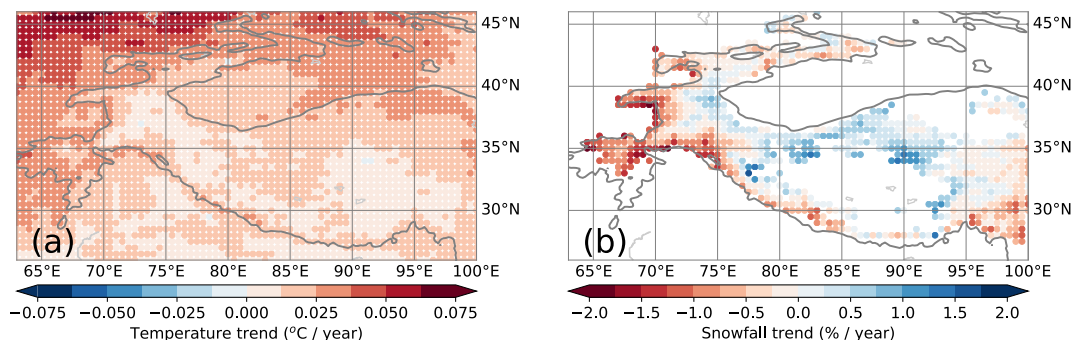
205

Figure 5: Trends between 1980-2010 of temperature in the melt season (a) and snowfall (b), averaged over 0.5x0.5° bins for clarity. Regions with monthly snowfall of less than 10 mm were masked out. The 2000 m elevation contour is indicated by a solid line.
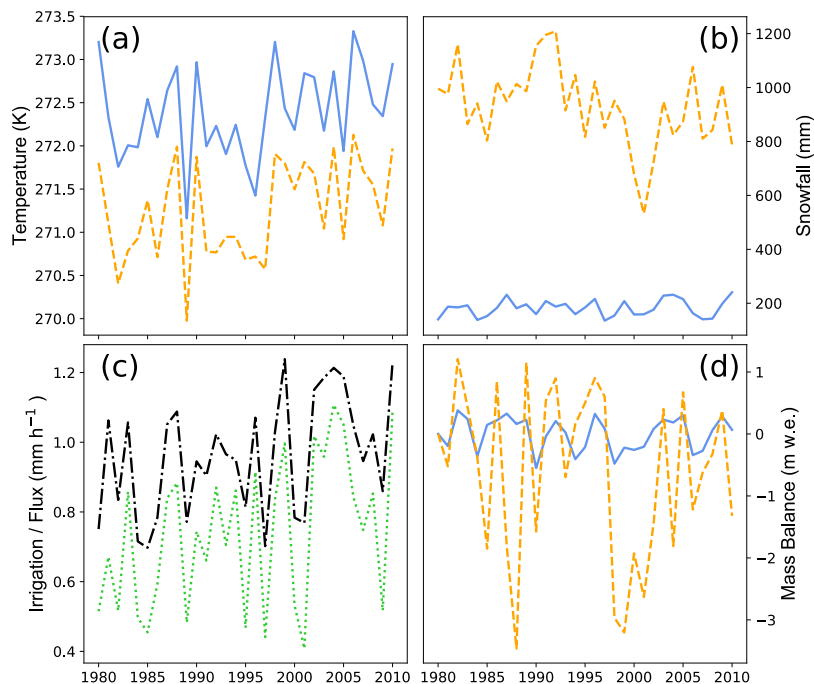

Figure 6: Time series of annual mean temperature (a), snowfall (b), mass balance (d) for representative 1x1° bins that have, on
210 **average, growing glaciers (38.5° N, 75.5° E, blue lines) and shrinking glaciers (34.5° N, 74.5° E, orange, dashed lines). Panel *c* shows**

the time series of annual irrigation gift (green, dotted line) and annual surface moisture flux (black, dot-dashed line) for the most heavily irrigated point in the Tarim.
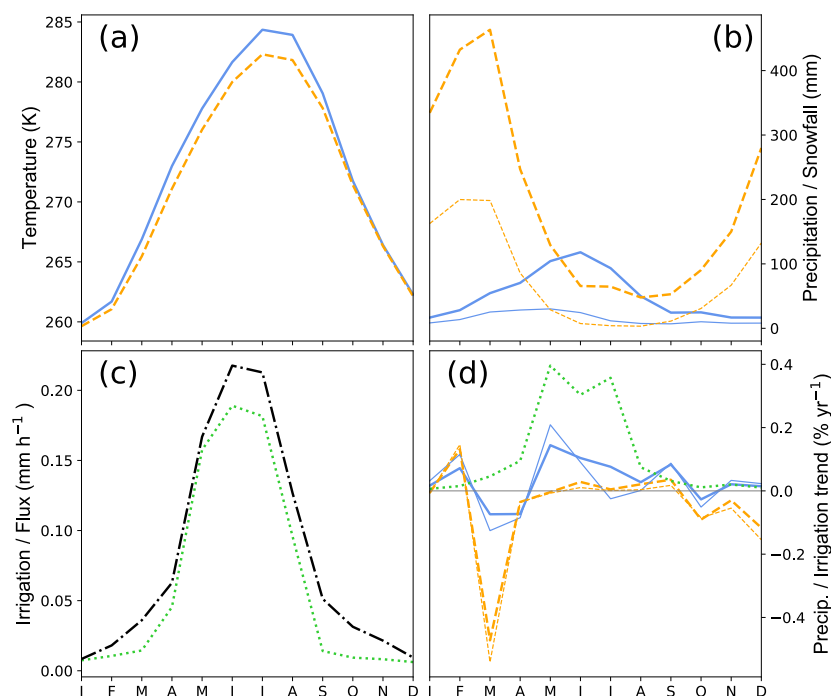

Figure 7: a) Mean seasonal cycle of temperature and b) precipitation (thick lines) and snowfall (think lines) between 1980-2010 for the WKSK (blue lines) and northwestern HMA (orange, dashed lines), as shown in Fig. 11b,d. c) Mean seasonal cycle of the irrigation gift (green, dotted line) and surface moisture flux (black, dot-dashed line) of the most heavily irrigated point in the Tarim. d) Trends in precipitation (thick lines) and snowfall (thin lines) for the WKSK (blue lines) and southwestern HMA (orange, dashed lines), and the trend in irrigation from the most heavily irrigated point in the Tarim (green, dotted line), all as percentages of the annual mean value.

Our trends show some similarities, but also major differences with respect to a similar WRF study that did not include irrigation and used another re-analysis dataset (Norris et al., 2018). For instance, our temperature trends do not exhibit the strong summer cooling at low altitudes (e.g. the Tarim basin), and are more in line with station data (Waqas & Athar, 2018; Xu, Liu, Fu, & Chen, 2010) in that respect.

3.3 Glacier mass balances

The resulting pattern of simulated mass balance (Fig. 8) shows a strong resemblance to the measured pattern of mass balances of recent decades. Most notably, we also obtain growing glaciers in WKSK, whereas the glaciers in other regions show large mass losses. In fact, all points where we model glacier growth in Fig. 3a also show growth or stable conditions in observations

230 (Brun et al., 2017; Kääb et al., 2015), except one point in Kääb et al., (2015). A more detailed quantitative comparison of the above results and the observed mass balances is hampered by the fact that our simulations only go out to 2010, but we compare our results for the period 2000-2008 in Fig. 9. The results generally match reasonably well, although our model seems to show too little growth for the growing glaciers. However, note that the errors on these observations (Brun et al., 2017) are large (~0.3 m w.e.). Furthermore, both the climate model and the glacier model will be associated with errors. By modulating the

235 initial mass balance in the model, we find that on average 41% of the modelled mass balance in 2010 is determined by the initial mass balance in 1980. Although the mass balances in 1980 were observed to be less extreme than in the 21st century (Bolch et al., 2012; Maurer, Schaefer, Rupper, & Corley, 2019), parts of HMA already had negative mass balances then, with the magnitude of initial mass balances generally less than 0.4 m w.e. yr^{-1}. This would result in an error on the mass balances in Fig. 8 of less than 0.2 m w.e. yr^{-1}. Despite these uncertainties, our results clearly show that the climatic change of the recent

240 decades has favoured growth of the glaciers in the regions where actual growth is observed, and not in the places where glaciers are melting fastest.
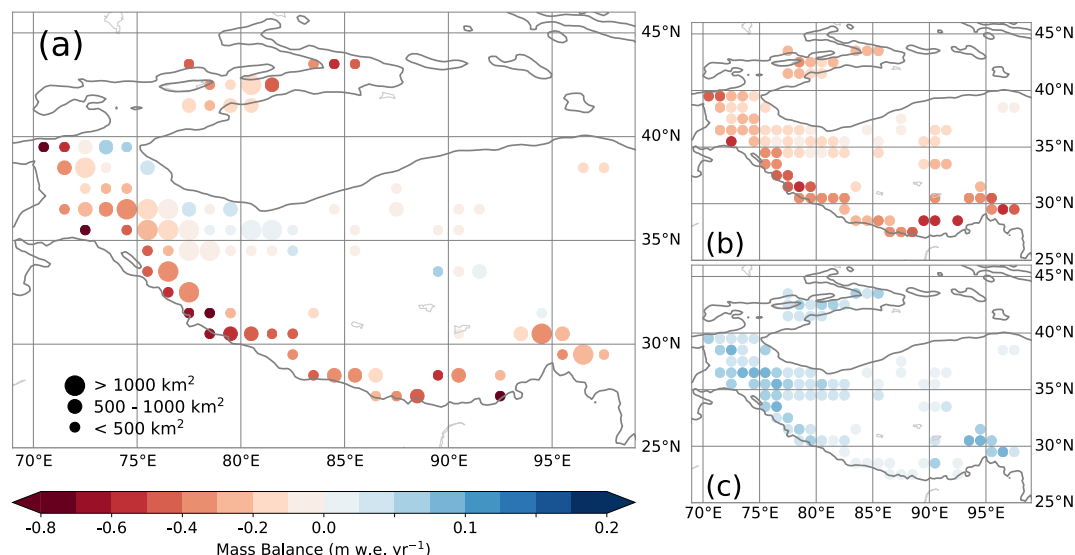
**Figure 8: Simulated mean mass balance between 2000-2010 forced by changes in temperature and snowfall from WRF (a), only
changes in temperature from WRF (b), and only changes in snowfall from WRF (c). Results are binned in 1x1° bins, and bins with
total glacier volumes less than 5 km^3 are not shown, to enable comparison with previous studies. The 2000 m elevation contour is
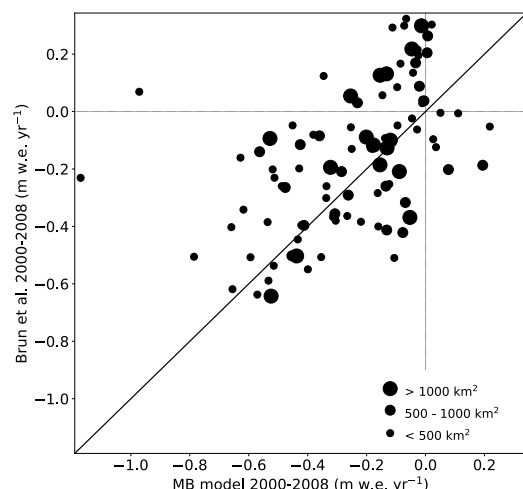indicated by a solid line.**

**Figure 9: Comparison between mean modelled mass balances from this work, binned on a 1x1° grid as in Fig. 8, and those derived
from observations of Brun et al. (2017), which are on the same grid, between 2000-2008.**

We also ran the glacier mass balance model forced by changes in temperature or snowfall only, to disentangle the model
sensitivities of the two different variables on the glacier mass balances (Figures 8b and 8c). These results show that the glaciers
in the western and southern HMA mainly lose mass due to the increase in temperature, whereas the changes in precipitation
have only a minor effect. On the other hand, in the regions where the glaciers are growing, the glaciers are barely affected by
the temperature increases in our model. The glacier growth in these regions is mainly caused by an increase in snow (Fig. 8c).
Furthermore, the increase in snow is possibly also responsible for moderating the temperature increases due to the high albedo
of fresh snow, which leads to less energy being used for melt. However, the weak temperature response in WKSK is not only
caused by the limited temperature trends, but is also due to the limited glacier temperature sensitivity there. We demonstrate
this by forcing the glacier model with uniform temperature and precipitation trends (Fig. 10). The reduced temperature
sensitivity is in line with previous work (Sakai & Fujita, 2017; Wang, Liu, Shangguan, Radic, & Zhang, 2019). The decrease
in snowfall in the western and southern HMA has a far smaller impact on the mass balance than the increase in temperature.
Especially the Himalaya show a low sensitivity to precipitation (Fig. 10). To be able to model thousands of glaciers, our mass
balance model is relatively simple and does not solve the full energy balance. A full energy balance model at 1 km resolution
has shown that the temperature increases can amplify melt in the monsoon-dominated Himalaya, whereas snowfall increases

13

in the melt season can amplify glacier growth in the Karakoram (Bonekamp, de Kok, Collier, & Immerzeel, 2019). Hence, more detailed models will likely strengthen our conclusion that the observed mass gains are caused by snow increases, whereas the observed mass losses are mainly caused by temperature increases. Unfortunately, modelling the climate and glaciers of the entire HMA at a sub-kilometre resolution for 30 years is currently beyond our capabilities.
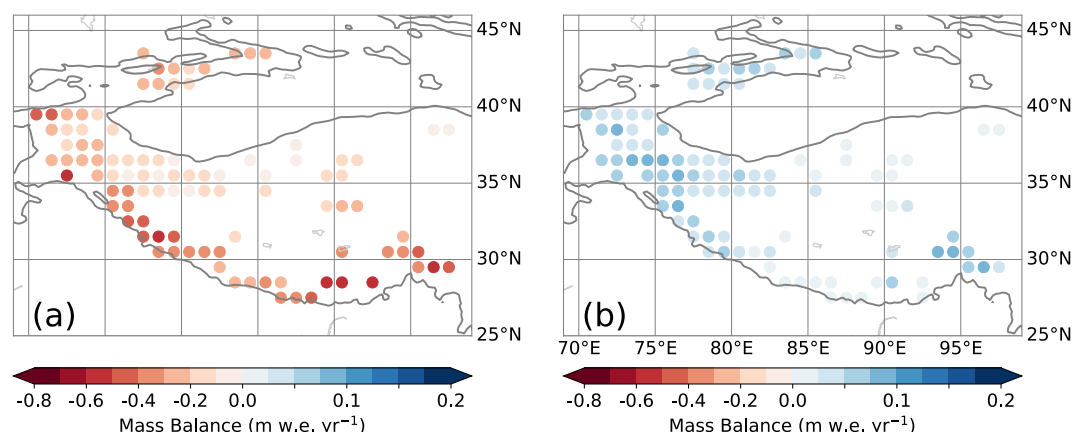
270

Figure 10: Simulated mean mass balance between 2000-2010 forced by a spatially uniform and constant temperature increase of +0.01 °C yr⁻¹, with snowfall kept constant (a), and a spatially uniform and constant snowfall increase of +0.5% yr⁻¹ of the annual mean value (b). Panels *a* and *b* thus show the relative sensitivity to temperature and snowfall, respectively.

275 ### 3.4 Moisture sources

The trends in moisture source regions for WKSK (Fig. 11a,b) indicate that the largest increases in moisture from a given source to precipitation in WKSK occur in the mountains themselves. This increase in recycling occurs mainly in May, and is also the main cause of the increase in precipitation in September (see Fig. 12). The increase in recycling is probably a natural consequence of the increased precipitation there. The regions with the second largest increases are the irrigated areas in the

280 Tarim basin, which contributes mainly in May-July (see Figs. 7 and 12). In July, the increase in Tarim irrigation still contributes to increasing precipitation in WKSK, but it falls more in the form of rain, compared to May, where it is mainly snow (Fig. 7). Another region that contributes to the increase in precipitation in WKSK is the Junggar basin, northeast of the Tarim basin. This is another arid region that has experienced rapid increases in irrigation. The increases per grid point are lower there, but spread out over a larger area. A final source region with an overall large positive trend is the Caspian Sea and the Caucasus.

285 Note again that, due to a systematic offset in surface moisture flux between WRF and ERA-Interim, the moisture source trends in the Tarim and HMA are underestimated with respect to the other regions.
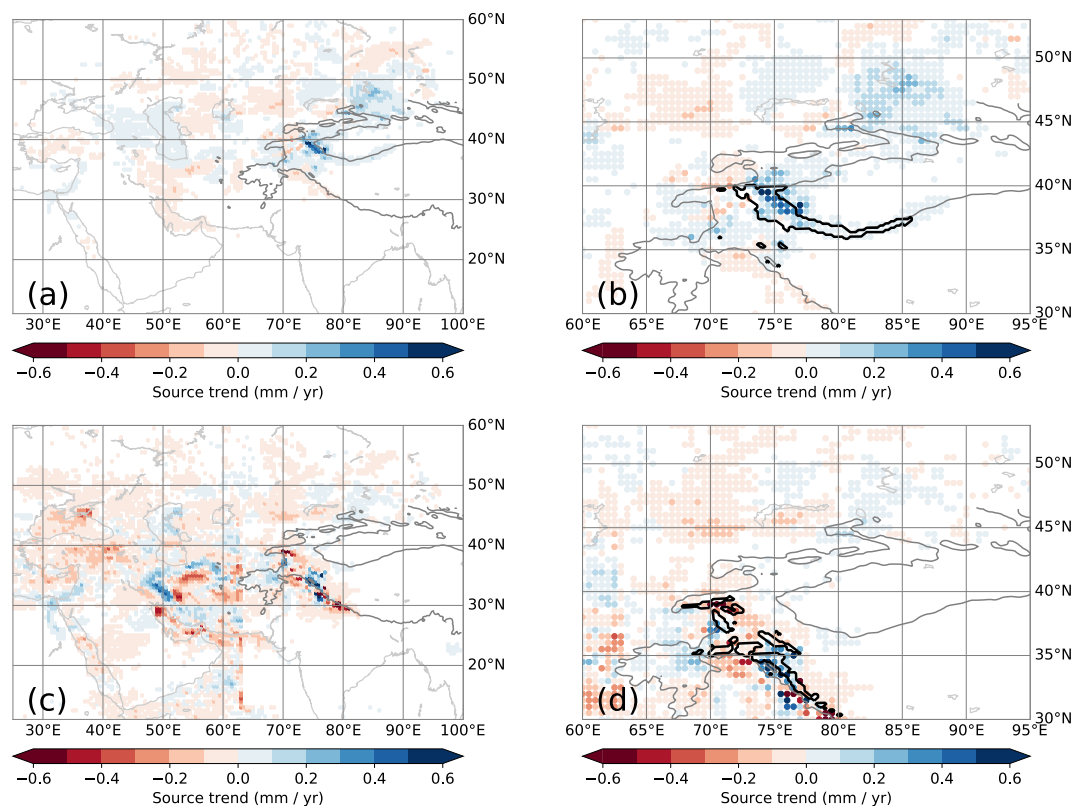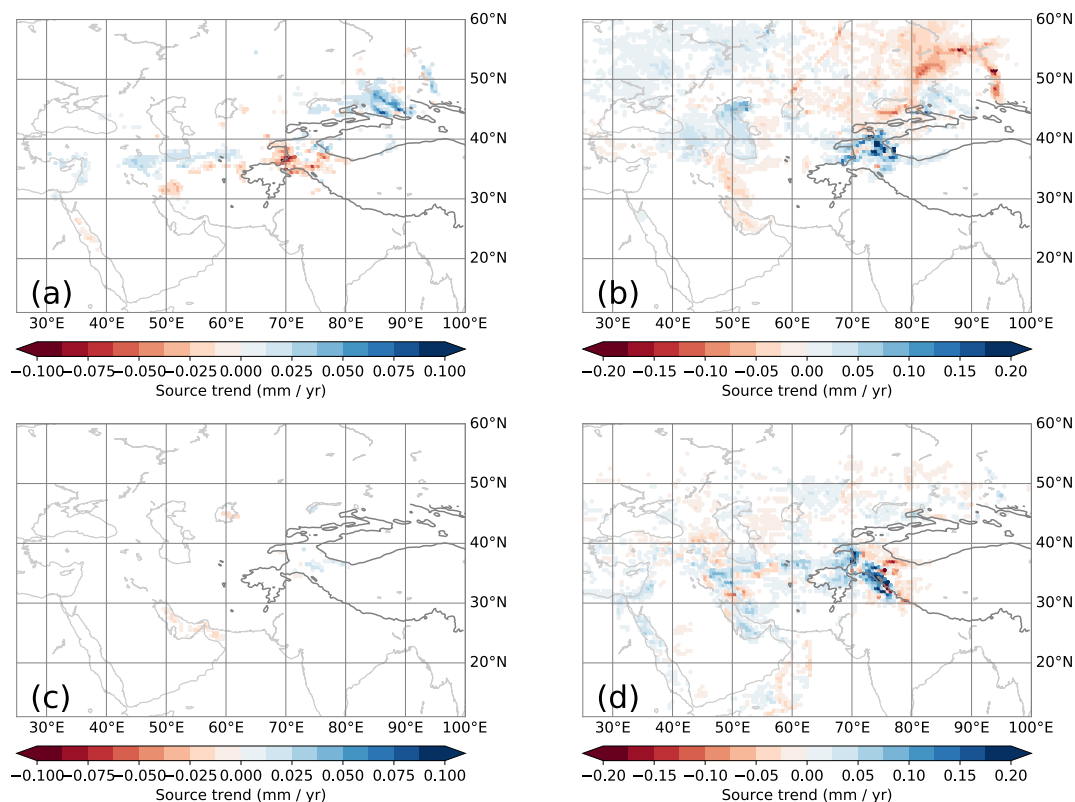
Figure 11: Trends in the amount of moisture from a given source contributing to precipitation trends in the target area (a,c), with a detailed view (b,d) around the target area from which the parcels were released (contoured in bold) for WKSK (a,b) and southwestern HMA (c,d). Trends with magnitudes smaller than 0.02 mm yr⁻¹ are made white. The 2000 m elevation contour in the WRF domain is indicated by a solid line.

290

15

Figure 12: Trends in the amount of moisture from a given source for WKSK for March (a), May (b), September (c) and for
295 **northwestern HMA in March (d). These months correspond to large negative or positive trends in snowfall in Fig. 7. Note the different scales.**

These results imply that evapotranspiration from irrigated areas in arid Northwest China play a large role in adding water to parts of HMA and hence to the observed positive mass balances. This is in line with recent work that shows that the recent
300 wetting of Central Asia and the Tarim basin is associated with an increase in evapotranspiration in these regions (Dong et al., 2018; Peng & Zhou, 2017; Peng, Zhou, Zhang, & Wu, 2018). The increase in the total evapotranspiration is influenced by the increase in potential evapotranspiration (Fang, Chen, & Li, 2018), increase in water availability (Jian et al., 2018), and increase in irrigated land area. On the interannual timescale, precipitation in WKSK strongly correlates with the moisture source amount in the western Tarim basin (Pearson r=0.96 below 3500 m, r=0.68 for the entire WKSK, as indicated in Fig. 11b). A similar
305 correlation exists between the WKSK precipitation and the Caspian Sea moisture source amount (r=0.89 below 3500 m, r=0.43

16

The Cryosphere
Discussions
Open Access
EGU

for the entire WKSK), showing the importance of the large-scale weather patterns. For the Junggar basin, this correlation is weaker (r=0.65 below 3500 m, r=-0.14 for the entire WKSK), since this region contributes in winter (Fig. 12).

310   When performing the moisture tracking for the southwestern part of HMA, where snowfall has generally decreased (Fig. 11c,d), also the Caspian Sea and the Junggar basin positively contribute to the snowfall trend, whereas for these ranges the Tarim basin does not contribute to the snowfall trend, with maximal trends in moisture sources of less than 0.1 mm yr^{-1}. These results show that the irrigated areas in the Tarim basin are especially important in influencing the moisture supply to the Western Kunlun Shan (de Kok et al., 2018).

4. Conclusion and discussion

315   Our simulations, based on ERA-Interim and GLDAS reanalysis data, indicate that an increase of snowfall and a low temperature sensitivity are the main reasons why glaciers are growing or stable in western Kunlun Shan and Karakoram. This is the first time that the observed pattern of glacier mass balances in HMA is reproduced in a consistent way. Although the interannual variability of temperature and precipitation is reasonably reproduced, our models are associated with uncertainties, which are partly irreconcilable due to a lack of *in situ* measurements in WKSK. Furthermore, different parameterisations in

320   the regional climate model, different irrigation schemes, and different glacier models will likely yield slightly different results. Using an ensemble of such approaches could be used to assess the robustness of the results presented here in the future. Furthermore, detailed studies at smaller scales will give more insight into individual glacier behaviour.

We show that the growing irrigated area in the arid region of Northwest China plays an important role in the increase in
325   snowfall in WKSK. Previous studies have already shown that increases of irrigation in Northwest China can add precipitation to neighbouring mountains (Cai et al., 2019; de Kok et al., 2018), but we now show this process of increasing irrigation is also important compared to other changes in the atmosphere over the last few decades. Already before 1980, irrigation has increased in Northwest China (Fang et al., 2018), possibly contributing to the stable glacier conditions then. Future evolution of snowfall in this part of HMA is partly linked to how the irrigated areas develop in the future. Changes in temperature, irrigated area, or
330   irrigation efficiency are therefore important parameters in understanding future run-off from glaciers and snow in WKSK. The increase in water availability for irrigation in Northwest China might be partly the result of the loss of glacier mass in Tien Shan (Dong et al., 2018). The mass loss will first result in an increase in glacier melt run-off into the Tarim basin, but ultimately the run-off will decrease as the glaciers shrink to a small size (Kraaijenbrink et al., 2017). On the other hand, if the primary source of irrigation water is groundwater, the amount of irrigation for the region will also have a limited sustainable or
335   economic level. Once the groundwater is depleted, the glaciers in WKSK will also receive less snowfall from this region, resulting in their retreat. The relative importance of groundwater extraction, melt from Tien Shan, and recycling from WKSK, for water availability in the Tarim is yet unknown and will require future study. Furthermore, improving the estimates of

The Cryosphere
Discussions

irrigation gifts, e.g. by remote sensing, could also improve the past climate reconstruction of WKSK. Greening and warming in West-Asia could provide additional snowfall to WKSK, together with an increase in westerly disturbances (Cannon et al.,

340 2014; Kapnick et al., 2014), but if temperatures in HMA keep increasing, the increase in melt will probably counteract glacier growth in most of HMA in the long term. It is clear that the coupling between glacier mass balance, runoff, and irrigation in different regions creates a complex problem of water availability, which will need to be researched further to inform decision makers on irrigation policies.

Acknowledgements

Code and data availability

The data underlying our results in Figs. 5-12, i.e. monthly mean output from WRF of temperature and precipitation, annual glacier mass balances, and annual moisture sources, will be directly accessible at *dataverse.nl* (https://hdl.handle.net/10411/ATONZD). Other data is available from the authors upon request. WRF and the glacier mass

355 balance model are freely available. The moisture tracking model is available upon request from Obbe A. Tuinenburg.

Author contributions

R.J.d.K. and W.W.I. designed the study, with input from all authors. R.J.d.K. performed the WRF modelling, P.D.A.K. performed the glacier mass balance modelling, and O.A.T. performed the moisture tracking. All authors contributed to the writing and editing of the manuscript.

360 **Competing interests**

The authors declare that they have no conflict of interest.

The Cryosphere
Discussions
Open Access
EGU

References

Beljaars, A. C. M.: The parametrization of surface fluxes in large???scale models under free convection. *Quarterly Journal of the Royal Meteorological Society*, *121*(522), 255–270. https://doi.org/10.1002/qj.49712152203, 1995.

365 Bocchiola, D., and Diolaiuti, G.: Recent (1980-2009) evidence of climate change in the upper Karakoram, Pakistan. *Theoretical and Applied Climatology*, *113*(3–4), 611–641. https://doi.org/10.1007/s00704-012-0803-y, 2013.

Bolch, T., Kulkarni, A., Kaab, A., Huggel, C., Paul, F., Cogley, J. G., Frey, H., Kargel, J.S., Fujita, K., Scheel, M., Bajrachatya, S., and Stoffel, M.:. The State and Fate of Himalayan Glaciers. *Science*, *336*(6079), 310–314. https://doi.org/10.1126/science.1215828, 2012.

370 Bonekamp, P., de Kok, R., Collier, E., and Immerzeel, W.: Contrasting meteorological drivers of the glacier mass balance between the Karakoram and central Himalaya. *Frontiers in Earth Science, in press*. https://doi.org/doi: 10.3389/feart.2019.00107, 2019.

Brun, F., Berthier, E., Wagnon, P., Kääb, A., and Treichler, D.: A spatially resolved estimate of High Mountain Asia glacier mass balances from 2000 to 2016. *Nature Geoscience*, *10*(9), 668–673. https://doi.org/10.1038/ngeo2999, 2017.

Cai, P., Luo, G., He, H., Zhang, M., and Termonia, P.: Agriculture intensification increases summer precipitation in Tianshan. *Atmospheric Research*, *227*(April), 140–146. https://doi.org/10.1016/j.atmosres.2019.05.005, 2019.

375 Cannon, F., Carvalho, L. M. V., Jones, C., and Bookhagen, B.: Multi-annual variations in winter westerly disturbance activity affecting the Himalaya. *Climate Dynamics*, *44*(1–2), 441–455. https://doi.org/10.1007/s00382-014-2248-8, 2014.

Collier, E., and Immerzeel, W. W.: High-resolution modeling of atmospheric dynamics in the Nepalese Himalayas. *Journal of Geophysical Research : Atmospheres*, *120*, 98822–99896. https://doi.org/10.1002/2015JD023266, 2015.

Cook, B. I., Shukla, S. P., Puma, M. J., and Nazarenko, L. S.: Irrigation as an historical climate forcing. *Climate Dynamics*, *44*(5–6), 1715–
380 1730. https://doi.org/10.1007/s00382-014-2204-7, 2015.

de Kok, R. J., Tuinenburg, O. A., Bonekamp, P. N. J., and Immerzeel, W. W.: Irrigation as a Potential Driver for Anomalous Glacier Behavior in High Mountain Asia. *Geophysical Research Letters*, *45*(4), 2047–2054. https://doi.org/10.1002/2017GL076158, 2018.

Dee, D. P., Uppala, S. M., Simmons, A. J., Berrisford, P., Poli, P., Kobayashi, S., Andrae, U., Balmaseda, M.A., Balsamo, G., Bauer, P., Bechtold, P., Beljaars, A.C.M., van de Berg, L., Bidlot, J., Bormann, N., Delsol, C., Dragani, R., Fuentes, M., Geer, A.J., Haimberger,
385 L., Healy, S.B., Hersbach, H., Hólm, E.V., Isaksen, L., Kållberg, P., Köhler, M., Matricardi, M., McNally, A.P., Monge-Sanz, B.M., Morcrette, J.-J., Park, B.-K., Peubey, C., de Rosnay, P., Tavolato, C., Thépaut, J.-N., and Vitart, F.: The ERA-Interim reanalysis: Configuration and performance of the data assimilation system. *Quarterly Journal of the Royal Meteorological Society*, *137*(656), 553–597. https://doi.org/10.1002/qj.828, 2011.

Dehecq, A., Gourmelen, N., Gardner, A. S., Brun, F., Goldberg, D., Nienow, P. W., Berthier, E., Vincent, Ch., Wagnon, P., and Trouvé, E.
390 : Twenty-first century glacier slowdown driven by mass loss in High Mountain Asia. *Nature Geoscience*, *12*, 22–27. https://doi.org/10.1038/s41561-018-0271-9, 2019.

Dlugokencky, E., Lang, P., Mund, J., Crotwell, M., and Thoning, K.: Atmospheric Carbon Dioxide Dry Air Mole Fractions from the NOAA ESRL Carbon Cycle Cooperative Global Air Sampling Network, 1968-2017, 2018..

Dong, W., Lin, Y., Wright, J. S., Xie, Y., Ming, Y., Zhang, H., Chen, R., Chen, Y., Xu, F., Lin, N., Yu, C., Zhang, B., Jin, S., Yang, K., Li,
395 Z., Guo, J., Wang, L., and Lin, G.: Regional disparities in warm season rainfall changes over arid eastern – central Asia. *Scientific Reports*, *8*(August), 13051. https://doi.org/10.1038/s41598-018-31246-3, 2018.

Dyer, A. J., and Hicks, B. B.: Flux- gradient relationships in the constant flux layer. *Quarterly Journal of the Royal Meteorological Society*, *96*(410), 715–721. https://doi.org/10.1002/qj.49709641012, 1970.

Fang, G., Chen, Y., and Li, Z.: Variation in agricultural water demand and its attributions in the arid Tarim River Basin. *The Journal of*
400 *Agricultural Science*, *156*(3), 301–311. https://doi.org/10.1017/S0021859618000357, 2018.

The Cryosphere
Discussions

Open Access

EGU

Forsythe, N., Fowler, H. J., Li, X.-F., Blenkinsop, S., and Pritchard, D.: Karakoram temperature and glacial melt driven by regional atmospheric circulation variability. *Nature Climate Change*, (August). https://doi.org/10.1038/nclimate3361, 2017.

Fowler, H. J., and Archer, D. R.: Conflicting signals of climatic change in the upper Indus Basin. *Journal of Climate*, *19*(17), 4276–4293. https://doi.org/10.1175/JCLI3860.1, 2006.

405 Gardelle, J., Berthier, E., and Arnaud, Y.: Slight mass gain of Karakoram glaciers in the early twenty-first century. *Nature Geoscience*, *5*(5), 322–325. https://doi.org/10.1038/ngeo1450, 2012.

Gardelle, J., Berthier, E., Arnaud, Y., and Kääb, A.: Region-wide glacier mass balances over the Pamir-Karakoram-Himalaya during 1999-2011. *Cryosphere*, *7*(4), 1263–1286. https://doi.org/10.5194/tc-7-1263-2013, 2013.

Hewitt, K.: The Karakoram Anomaly? Glacier Expansion and the 'Elevation Effect,' Karakoram Himalaya. *Mountain Research and*
410 *Development*, *25*(4), 332–340. https://doi.org/10.1659/0276-4741(2005)025[0332:TKAGEA]2.0.CO;2, 2005.

Hong, S.-Y., Noh, Y., and Dudhia, J.: A new vertical diffusion package with an explicit treatment of entrainment processes. *Monthly Weather Review*, *134*(9), 2318–2341. https://doi.org/10.1175/MWR3199.1, 2006.

Iacono, M. J., Delamere, J. S., Mlawer, E. J., Shephard, M. W., Clough, S. A., and Collins, W. D.: Radiative forcing by long-lived greenhouse gases: Calculations with the AER radiative transfer models. *Journal of Geophysical Research Atmospheres*, *113*(13), 2–9.
415 https://doi.org/10.1029/2008JD009944, 2008.

Immerzeel, W. W., Wanders, N., Lutz, A. F., Shea, J. M., and Bierkens, M. F. P.: Reconciling high-altitude precipitation in the upper Indus basin with glacier mass balances and runoff. *Hydrology and Earth System Sciences*, *19*(11), 4673–4687. https://doi.org/10.5194/hess-19-4673-2015, 2015.

Jian, D., Li, X., Sun, H., Tao, H., Jiang, T., Su, B., and Hartmann, H.: Estimation of Actual Evapotranspiration by the Complementary
420 Theory-Based Advection–Aridity Model in the Tarim River Basin, China. *Journal of Hydrometeorology*, *19*(2), 289–303. https://doi.org/10.1175/JHM-D-16-0189.1, 2018.

Kääb, A., Treichler, D., Nuth, C., and Berthier, E.: Brief Communication: Contending estimates of 2003-2008 glacier mass balance over the Pamir-Karakoram-Himalaya. *Cryosphere*, *9*(2), 557–564. https://doi.org/10.5194/tc-9-557-2015, 2015.

Kain, J. S.: The Kain–Fritsch Convective Parameterization: An Update. *Journal of Applied Meteorology*, *43*(1), 170–181.
425 https://doi.org/10.1175/1520-0450(2004)043<0170:TKCPAU>2.0.CO;2, 2004.

Kapnick, S. B. S., Delworth, T. L. T., Ashfaq, M., Malyshev, S., and Milly, P. C. D.: Snowfall less sensitive to warming in Karakoram than in Himalayas due to a unique seasonal cycle. *Nature Geoscience*, *7*(11), 834–840. https://doi.org/10.1038/ngeo2269, 2014.

Khattak, M. S., Babel, M. S., and Sharif, M.: Hydro-meteorological trends in the upper Indus River basin in Pakistan. *Climate Research*, *46*(2), 103–119. https://doi.org/10.3354/cr00957, 2011.

430 Kraaijenbrink, P. D. A., Bierkens, M. F. P., Lutz, A. F., and Immerzeel, W. W.: Impact of a global temperature rise of 1.5 degrees Celsius on Asia's glaciers. *Nature*, *549*(7671), 257–260. https://doi.org/10.1038/nature23878, 2017.

Lawrimore, J. H., Menne, M. J., Gleason, B. E., Williams, C. N., Wuertz, D. B., Vose, R. S., and Rennie, J.: Global Historical Climatology Network - Monthly (GHCN-M), Version 3. https://doi.org/10.7289/V5X34VDR, 2011.

Lee, E., Sacks, W. J., Chase, T. N., and Foley, J. A.: Simulated impacts of irrigation on the atmospheric circulation over Asia. *Journal of*
435 *Geophysical Research Atmospheres*, *116*(8), 1–13. https://doi.org/10.1029/2010JD014740, 2011.

Lin, H., Li, G., Cuo, L., Hooper, A., and Ye, Q.: A decreasing glacier mass balance gradient from the edge of the Upper Tarim Basin to the Karakoram during 2000 – 2014. *Scientific Reports*, (December 2016), 1–9. https://doi.org/10.1038/s41598-017-07133-8, 2017.

Lobell, D. B., Bonfils, C., and Faurès, J. M.: The role of irrigation expansion in past and future temperature trends. *Earth Interactions*, *12*(3), 1–11. https://doi.org/10.1175/2007EI241.1, 2008.

440 Martens, B., Miralles, D. G., Lievens, H., Van Der Schalie, R., De Jeu, R. A. M., Fernández-Prieto, D., Beck, H.E., Dorigo, W.A., Verhoest, N. E. C.: GLEAM v3: Satellite-based land evaporation and root-zone soil moisture. https://doi.org/10.5194/gmd-10-1903-2017, 2017.

Maurer, J. M., Schaefer, J. M., Rupper, S., and Corley, A.: Acceleration of ice loss across the Himalayas over the past 40 years. *Science Advances*, 5, 1–12. https://doi.org/10.1126/sciadv.aav7266, 2019.

Ménégoz, M., Gallée, H., and Jacobi, H. W.: Precipitation and snow cover in the Himalaya : from reanalysis to regional climate simulation, 445 *Hydrology and Earth System Sciencs*, 17, 3921–3936. https://doi.org/10.5194/hess-17-3921-2013, 2013.

Miralles, D. G., Gash, J. H., Holmes, T. R. H., De Jeu, R. A. M., and Dolman, A. J.: Global canopy interception from satellite observations. https://doi.org/10.1029/2009JD013530, 2010.

Morrison, H., Thompson, G., and Tatarskii, V.: Impact of Cloud Microphysics on the Development of Trailing Stratiform Precipitation in a Simulated Squall Line: Comparison of One- and Two-Moment Schemes. *Monthly Weather Review*, 137(3), 991–1007. 450 https://doi.org/10.1175/2008MWR2556.1, 2009.

Niu, G. Y., Yang, Z. L., Mitchell, K. E., Chen, F., Ek, M. B., Barlage, M., Kumar, A., Manning, K., Niyogi, D., Rosero, W., Tewari, M., and Xia, Y. (2011). The community Noah land surface model with multiparameterization options (Noah-MP): 1. Model description and evaluation with local-scale measurements. *Journal of Geophysical Research Atmospheres*, 116(12), 1–19. https://doi.org/10.1029/2010JD015139, 2011.

455 Norris, J., Carvalho, L. M. V., Jones, C., and Cannon, F.: WRF simulations of two extreme snowfall events associated with contrasting extratropical cyclones over the western and central Himalaya. *Journal of Geophysical Research Atmospheres*, 120(8), 3114–3138. https://doi.org/10.1002/2014JD022592, 2015.

Norris, J., Carvalho, L. M. V., Jones, C., and Cannon, F.: Deciphering the contrasting climatic trends between the central Himalaya and Karakoram with 36 years of WRF simulations. *Climate Dynamics*, 52(0), 159. https://doi.org/10.1007/s00382-018-4133-3, 2018.

460 Otte, T. L., Nolte, C. G., Otte, M. J., and Bowden, J. H.: Does nudging squelch the extremes in regional climate modeling? *Journal of Climate*, 25(20), 7046–7066. https://doi.org/10.1175/JCLI-D-12-00048.1, 2012.

Palazzi, E., Von Hardenberg, J., and Provenzale, A.: Precipitation in the hindu-kush karakoram himalaya: Observations and future scenarios. *Journal of Geophysical Research Atmospheres*, 118(1), 85–100. https://doi.org/10.1029/2012JD018697, 2013.

Paulson, C. A.:. The Mathematical Representation of Wind Speed and Temperature Profiles in the Unstable Atmospheric Surface Layer. 465 *Journal of Applied Meteorology*, Vol. 9, pp. 857–861. https://doi.org/10.1175/1520-0450(1970)009<0857:TMROWS>2.0.CO;2, 1970.

Peng, D., and Zhou, T.: Why was the arid and semiarid Northwest China getting wetter in the recent decades? *Journal of Geophysical Research: Atmospheres*. https://doi.org/10.1002/2016JD026424, 2017.

Peng, D., Zhou, T., Zhang, L., and Wu, B.: Human Contribution to the Increasing Summer Precipitation in Central Asia from 1961 to 2013. 470 *Climate Dynamics*, 31, 8005–8021. https://doi.org/10.1175/JCLI-D-17-0843.1, 2018.

Pfeffer, W. T., Arendt, A. A., Bliss, A., Bolch, T., Cogley, J. G., Gardner, A. S., Hagen, J.-O., Hock, R., Kaser, G., Kienholz, Ch., Miles, E.S., Moholdt, G., Mölg, N., Paul, F., Radić, V., Rastner, P., Raup, B.H., Rich, J., Sharp, M.J., and The Randolph Consortium: The randolph glacier inventory: A globally complete inventory of glaciers. *Journal of Glaciology*, 60(221), 537–552. https://doi.org/10.3189/2014JoG13J176, 2014.

475 Prinn, R. G., Weiss, R. F., Simmonds, P. J. F. P. G., Cunnold, D. M., Alyea, F. N., Doherty, S. O., Salameh, P., Miller, B.R., Huang, J., Wang, R.H.J., Hartley, D.E., Harth, C., Steele, L.P., Sturrock, G., Midgley, P.M., and McCulloch, A.: A history of chemically and radiatively important gases in air deduced from ALE_GAGE_AGAGE. *Journal of Geophysical Research : Atmospheres*, 105(D14), 17,751-17,792, 2000.

Puma, M. J., and Cook, B. I.: Effects of irrigation on global climate during the 20th century. *Journal of Geophysical Research Atmospheres*, 480 115(16), 1–15. https://doi.org/10.1029/2010JD014122, 2010.

21

The Cryosphere
Discussions

Open Access

EGU

Rodell, M., Houser, P. R., Jambor, U., Gottschalck, J., Mitchell, K., Meng, C.-J., Arsenailt, K., Cosgrove, B., Radakovich, J., Bosilovich, M., Entin, J.K., Walker, J.P., Lohmann, D., and Toll, D.: The Global Land Data Assimilation System. *Bulletin of the American Meteorological Society*, *85*(3), 381–394. https://doi.org/10.1175/BAMS-85-3-381, 2004.

Sacks, W. J., Cook, B. I., Buenning, N., Levis, S., and Helkowski, J. H.: Effects of global irrigation on the near-surface climate. *Climate Dynamics*, *33*(2–3), 159–175. https://doi.org/10.1007/s00382-008-0445-z, 2009.

Sakai, A., and Fujita, K.: Contrasting glacier responses to recent climate change in high-mountain Asia. *Scientific Reports*, *7*(1), 13717. https://doi.org/10.1038/s41598-017-14256-5, 2017.

Senay, G. B.: Satellite psychrometric formulation of the operational simplified surface energy balance (SSEBOP) model for quantiying and mapping evapotranspiration, *Applied Engineering in Agriculture*, *34*(3), 555–566, 2018.

Siebert, S., Burke, J., Faures, J. M., Frenken, K., Hoogeveen, J., Döll, P., and Portmann, F. T.: Groundwater use for irrigation - A global inventory. *Hydrology and Earth System Sciences*, *14*(10), 1863–1880. https://doi.org/10.5194/hess-14-1863-2010, 2010.

Skamarock, W. C., and Klemp, J. B.: A time-split nonhydrostatic atmospheric model for weather research and forecasting applications. *Journal of Computational Physics*, *227*(7), 3465–3485. https://doi.org/10.1016/j.jcp.2007.01.037, 2008.

Tuinenburg, O. A., Hutjes, R. W. A., and Kabat, P.: The fate of evaporated water from the Ganges basin. *Journal of Geophysical Research Atmospheres*, *117*(1), 1–17. https://doi.org/10.1029/2011JD016221, 2012.

Ul Hasson, S., Böhner, J., and Lucarini, V.: Prevailing climatic trends and runoff response from Hindukush-Karakoram-Himalaya, upper Indus Basin. *Earth System Dynamics*, *8*(2), 337–355. https://doi.org/10.5194/esd-8-337-2017, 2017.

van Beek, L. P. H., and Bierkens, M. F. P.: The Global Hydrological Model PCR-GLOBWB: Conceptualization, Parameterization and Verification. *Utrecht University, Department of Physical Geography, Http://Vanbeek.Geo.Uu.Nl/Suppinfo/Vanbeekbierkens2009.Pdf.* Retrieved from http://vanbeek.geo.uu.nl/suppinfo/vanbeekbierkens2009.pdf, 2008.

van Beek, L. P. H., Wada, Y., and Bierkens, M. F. P.: Global monthly water stress: 1. Water balance and water availability. *Water Resources Research*, *47*(7). https://doi.org/10.1029/2010WR009791, 2011.

Van der Esch, S., Ten Brink, B., Stehfest, E., Bakkenes, M., Sewell, A., Bouwman, A., Meijer, J., Westhoek, and Van den Berg, M. (2017). Exploring future changes in land use and land condition and the impacts on food, water, climate change and biodiversity Scenarios for the UNCCD Global Land Outlook Policy Report. *PBL Report Http://Www.Pbl.Nl/Sites/Default/Files/Cms/Publicaties/Pbl-2017-Exploring-Future-Changes-in-Land-Use-and-Land-Condition-2076.Pdf.* Retrieved from http://www.pbl.nl/sites/default/files/cms/publicaties/pbl-2017-exploring-future-changes-in-land-use-and-land-condition-2076.pdf, 2017.

Wada, Y., Van Beek, L. P. H., Viviroli, D., Drr, H. H., Weingartner, R., and Bierkens, M. F. P.: Global monthly water stress: 2. Water demand and severity of water stress. *Water Resources Research*, *47*(7), 1–17. https://doi.org/10.1029/2010WR009792, 2011.

Wada, Y., Wisser, D., and Bierkens, M. F. P.: Global modeling of withdrawal, allocation and consumptive use of surface water and groundwater resources. *Earth System Dynamics*, *5*(1), 15–40. https://doi.org/10.5194/esd-5-15-2014, 2014.

Wang, R., Liu, S., Shangguan, D., Radic, V., and Zhang, Y.: Spatial Heterogeneity in Glacier Mass-Balance Sensitivity across High Mountain Asia. *Water*, *11*, 776. https://doi.org/10.3390/w11040776, 2019.

Waqas, A., and Athar, H.: Recent decadal variability of daily observed temperatures in Hindukush , Karakoram and Himalaya region in northern Pakistan. *Climate Dynamics*, *0*(0), 0. https://doi.org/10.1007/s00382-018-4557-9, 2018.

Webb, E. K.: Profile relationships: The log- linear range, and extension to strong stability. *Quarterly Journal of the Royal Meteorological Society*, *96*(407), 67–90. https://doi.org/10.1002/qj.49709640708, 1970.

Xu, Z., Liu, Z., Fu, G., and Chen, Y.: Trends of major hydroclimatic variables in the Tarim River basin during the past 50 years. *Journal of Arid Environments*, *74*(2), 256–267. https://doi.org/10.1016/j.jaridenv.2009.08.014, 2010.

22

Zhang, D., and Anthes, R. A.: A High-Resolution Model of the Planetary Boundary Layer—Sensitivity Tests and Comparisons with SESAME-79 Data. *Journal of Applied Meteorology*, Vol. 21, pp. 1594–1609. https://doi.org/10.1175/1520-0450(1982)021<1594:AHRMOT>2.0.CO;2, 1982.

525